Advances in Nano Research, *Vol. 5 No. 3 (2017) 215-230*
DOI: https://doi.org/10.12989/anr.2017.5.3.215

Synthesis, morphology and electrochemical applications of iron oxide based nanocomposites

Camila J. Letti [1], Karla A.G. Costa [2], Marcos A. Gross [2], Leonardo G. Paterno [2], Marcelo A. Pereira-da-Silva [3,4], Paulo C. Morais [1,5] and Maria A.G. Soler [*1]

[1] *Instituto de Fisica, Universidade de Brasilia, Brasilia-DF 70910-900, Brazil*
[2] *Instituto de Quimica, Universidade de Brasilia, Brasilia-DF 70910-900, Brazil*
[3] *Instituto de Fisica de São Carlos USP, São Carlos-SP 13560-970, Brazil*
[4] *Centro Universitario Central Paulista – UNICEP, São Carlos-SP 13563-470, Brazil*
[5] *Schol of Chemistry and Chemical Engineering, Anhui University, Hefei 230601, China*

(*Received December 06, 2016, Revised July 10, 2017, Accepted July 29, 2017*)

Abstract. The development of hybrid systems comprising nanoparticles and polymers is an opening pathway for engineering nanocomposites exhibiting outstanding mechanical, optical, electrical, and magnetic properties. Among inorganic counterpart, iron oxide nanoparticles (IONP) exhibit high magnetization, controllable surface chemistry, spintronic properties, and biological compatibility. These characteristics enable them as a platform for biomedical applications and building blocks for bottom-up approaches, such as the layer-by-layer (LbL). In this regard, the present study is addressed to investigate IONP synthesised through co-precipitation route (average diameter around 7 nm), with either positive or negative surface charges, LbL assembled with sodium sulfonated polystyrene (PSS) or polyaniline (PANI). The surface and internal morphologies, and electrochemical properties of these nanocomposites were probed with atomic force microscopy, UV-vis and Raman spectroscopy, scanning electron microscopy, cross-sectional transmission electron microscopy, and electrochemical measurements. The nanocomposites display a globular morphology with IONP densely packed while surface dressed by polyelectrolytes. The investigation of the effect of thermal annealing (300 up to 600℃) on the oxidation process of IONP assembled with PSS was performed using Raman spectroscopy. Our findings showed that PSS protects IONP from oxidation/phase transformation to hematite up to 400℃. The electrochemical performance of nanocomposite comprising IONP and PANI were investigated in 0.5 mol×L^{-1} Na_2SO_4 electrolyte solution by cyclic voltammetry and chronopotentiometry. Our findings indicate this structure as promising candidate for potential application as electrodes for supercapacitors.

Keywords: nanocomposite; iron oxide nanoparticles; nanostructured electrodes; oxidation; layer-by-layer; polyaniline; sulfonated polystyrene; supercapacitors

1. Introduction

The assembly of nanoobjects or "building blocks" already displaying useful functions, such as nanomagnets or nanosemiconductors, leads to new generations of multifunctional nanomaterials with interesting fundamental properties as well as promising applications, the latter running from spintronics to nanomedicine (Balazs *et al*. 2006, Alivisatos 1996, Bruchez *et al*. 1998, Grassian

*Corresponding author, Professor, E-mail: soler@unb.br

 ISSN: 2287-237X (Print), 2287-2388 (Online)

2008, Toulemon *et al*. 2016). Moreover, bottom-up approaches with advantages of cost effective, large area fabrication, simple processes and automation facilities, such as the layer-by-layer (LbL) (Decher 1997), allow designing of all-organic and organic–inorganic hybrid multilayers with nanometric control over morphology and architecture. Resulting nanohybrid structures not only combine attractive functionalities of each component but also show synergetic characteristics, as for instance nanohybrids comprising iron oxide superparamagnetic particles and polymers can display collective magnetic properties arising from inter-particle interactions (Soler *et al*. 2012a). In addition, the interface nanoparticle-polymer influences the electric properties (Alcantara *et al*. 2013a). Nanoparticle (NP) interactions depend on particle and polymer characteristics as well as particle spatial distribution and self-organization inside the matrix. Fine control of the film thickness and average particle-particle distance within the structure can be accomplished by varying the number of bilayers (iron oxide/polymer) or via changing the concentration of particles within the colloidal dispersion used for film fabrication (Paterno *et al*. 2009a). Indeed, post-treatment of the as-deposited NP layer with appropriated solutions can trigger layer self-organization in a well-controllable way (Xiang *et al*. 2016).

Among inorganic counterpart, iron oxide nanoparticles (IONP) have received a great deal of attention due to their unique characteristics such as superparamagnetism, biocompatibility and very controllable surface chemistry. Iron-based cubic ferrites present chemical composition MFe_2O_4, where M is a divalent transition-metal as for instance Fe, Co, Ni, Mn, Cu, Zn, and Cd (Soler and Paterno 2017). On the other hand, maghemite (γ-Fe_2O_3) is an iron-deficient cubic ferrite, which in addition to magnetite (Fe_3O_4) and cobalt-ferrite ($CoFe_2O_4$) is among the most investigated iron oxides. The crystal symmetry is cubic and corresponds to the space group $O_h^7(Fd3m)$. Further, magnetite is predicted having a half-metallic character with a large spin polarization at the Fermi level, displaying a high Curie temperature (850 K) and electrical resistivity of the same order of magnitude as a semiconductor, thus being a promising candidate for spintronic applications. In addition, IONP systems can be synthesized through easy up-scaling and cost-effective chemical routes allowing fine size control, size distribution, shape, crystallinity, and stability.

IONP systems can be exploited in a variety of applications (Philip and Laskar 2012), such as biomolecular separation (Magnani *et al*. 2006), nanocatalysis (Dalpozzo 2015), rotating seals and magnetorheological vibration dampers (Marinică *et al*. 2016), SERS probe (Sun *et al*. 2016), insulating oil for improvement of transformer's cooling efficiency (Viali *et al*. 2010), sensors (Chen *et al*. 2013, Alcantara *et al*. 2013a, Santos *et al*. 2014, Wang *et al*. 2015, Aroutiounian *et al*. 2015), and biomedical applications (Trahms 2010, Ho *et al*. 2011, Thuy 2012, Gao *et al*. 2016, Zarrin *et al*. 2016). Very often, applications require spherical IONP core with diameter below 20 nm and functionalized with molecular coatings to promote the required colloidal stability, biocompatibility, and biological site targeting capability (Begin-Colin and Felder-Flesch 2012). Highly stable colloidal dispersions of IONP in a hosting carrier liquid are known as magnetic fluids (MF) or ferrofluids (Blums *et al*. 1985).

LbL assembly of magnetic nanofilms has been successfully prepared from colloidal IONP (magnetite, maghemite, or cobalt ferrite) and different polyelectrolytes, including conducting ones such as doped-polyaniline. Reported results accomplished fundamental studies regarding experimental and simulation of NP adsorption, NP oxidation, morphology, structure, optical, dielectric and magnetic properties of iron oxide based nanocomposites. (Correa-Duarte *et al*. 1998, Mamedov *et al*. 2000, Kim *et al*. 2002, Suda *et al*. 2005, Grigoriev *et al*. 2007, Paterno *et al*. 2009a, b, 2010, 2012, Pereira *et al*. 2010, Dey *et al*. 2010, Pichon *et al*. 2011, Alcantara *et al*.

2011a, b, Soler *et al*. 2012a, Neumann *et al*. 2013, Ko *et al*. 2015, Letti *et al*. 2017). In addition, the superparamagnetic behavior of the iron oxide nanoparticles is maintained when they are assembled layer-by-layer with either PANI or PSS polymer matrixes (Paterno *et al*. 2010). Indeed, the magnetic saturation displayed by nanofilms are similar to that measured in the powder samples of iron oxide employed as source of nanoparticle in the layer-by-layer assembly (Soler *et al*. 2012b). Moreover, recent reports have emphasized LbL-assembled iron oxide structures for potential applications beyond the superparamagnetic behavior. The presence of Fe^{2+} and Fe^{3+} ions enables iron oxide nanoparticles for a variety of electrochemical devices, including capacitor electrodes (Alcantara *et al*. 2013a) and chemical sensors (Santos *et al*. 2014, Alcantara *et al*. 2013b).

In the present contribution, we report on the preparation of two types of nanocomposites comprising IONP and sodium sulfonated polystyrene (PSS) or polyaniline (PANI). These nanocomposites were characterized by atomic force microscopy (AFM), UV-vis and Raman spectroscopy, scanning electron microscopy (SEM) and transmission electron microscopy (TEM). PSS-based nanocomposites were employed as a model system to study the oxidation process of IONP embedded into the PSS matrix, under air atmosphere, in the temperature range from 300 to 600℃. Moreover, the electrochemical behavior of (PANI/IONP@cit) nanocomposite films was investigated aiming to probe its supercapacitive performance.

2. Materials and methods

2.1 Materials

$FeCl_2.4H_2O$, $FeCl_3.6H_2O$, NaOH, $HClO_4$, 3-mercapto propanesulfonic acid sodium salt (3-MPS), sodium sulfonated polystyrene PSS (Mw 70,000 g×mol^{-1}), and PANI (Mw 10,000 g×mol^{-1}) were purchased from Sigma-Aldrich (Brazil). All chemicals were analytical grade or better and used as received. Nanocomposite films were deposited onto plain and Gold-platted (200 nm) optical glass slides (25 × 10 × 1 mm) and Indium-doped tin oxide (ITO) substrates (25 × 10 × 1 mm; sheet resistance: 15 ohm-square). The plain substrates were cleaned in piranha (H_2SO_4/H_2O_2, 3:1, v/v) and RCA ($H_2O/NH_4OH/H_2O_2$, 3:1:1, v/v) solutions as described elsewhere (Paterno *et al*. 2009a). Gold-platted substrates were soaked overnight into 3-MPS aqueous solution (20 mmol×L^{-1}) (Alcantara et *al*. 2011a). In both treatments, substrates become negatively-charged as required for the electrostatic driven film assembly. All experiments used exclusively ultra-pure water (18 MOhm×cm^{-1}) provided by a Milli-Q Millipore water purification system.

2.2 Synthesis of iron oxide nanoparticles

Hydrothermal (Kurtinaitienė *et al*. 2016) and co-precipitation (Soler *et al*. 2007, Butt and Jafri 2015) are the most employed methods to synthesize IONP. The co-precipitation method for synthesizing MFe_2O_4-based nanoparticles usually employs acid aqueous solutions of M^{2+} and Fe^{3+} ions for further reaction with a selected alkaline aqueous solution, as for instance $M^{2+} = Co^{2+}$ (Fe^{2+}) if cobalt ferrite (magnetite) is aimed to be produced. In both cases, the molar Co^{2+}/Fe^{3+} (Fe^{2+}/Fe^{3+}) ratio is fixed at 1:2 (Kang *et al*. 1996, Soler *et al*. 2005). Shortly, the mechanism proposed for this reaction is that the alkaline hydrolysis is responsible for the formation of hydroxylated metal ion complexes. Then, individual hydroxylated complexes are connected via condensation reactions, which lead to the formation of iron oxide solid networks. Since the hydroxylation step is pH

dependent, the size and shape of the solid is extremely sensitive to pH conditions (Jolivet *et al*. 2010). In aqueous-based media the IONP surface is stabilized and terminated with oxyhydroxyl groups (Schwertmann and Cornell 1991) and therefore protonation-deprotonation equilibrium is easily shifted by varying pH conditions in the media (Massart *et al*. 1995). The stability of aqueous-based IONP suspensions is higher in low or high pH values; the nanoparticle's surface becomes positively-charged (low pH) or negatively-charged (high pH) due to protonation or de-protonation, respectively (Qu and Morais 2000) and colloidal stability is achieved through inter-particle electrostatic repulsion. In low pH condition, IONP behave as cations and can thus be assembled with several polyanions via the LbL technique. Colloidal stabilization can also be achieved by steric repulsion when the suspended nanoparticles are surface-coated with molecules having high affinity with the carrier liquid. Likewise, electrostatic plus steric repulsion may work together against nanoparticle clustering when IONP surface complexation is realized using a molecular polyfunctional ligand, allowing dispersion of the IONP in aqueous medium (Soler and Paterno 2017). These systems, comprising an IONP core surface-functionalized with positively- or negatively-ionized functional groups are able to attach to a pay load, and can be dispersed in adequate pH to be employed as a platform for biomedical applications and building blocks for bottom-up approaches such as the LbL assembly (Soler *et al*. 2011).

Nanosized magnetite was synthesized according to the procedure described elsewhere (Kang *et al*. 1996). In short, the procedure consisted on adding, dropwise, a mixed solution of Fe^{2+} (0.05 mol×L^{-1}) and Fe^{3+} (0.1 mol×L^{-1}) to a magnetic stirred NaOH (0.4 mol×L^{-1}) solution. After addition of the iron-containing ions solution into the alkaline solution, the reaction mixture was magnetically stirred for 30 min more. The black solid precipitate of magnetite nanoparticles formed thereafter was washed several times with water and separated with a magnet. A colloidal dispersion was prepared by dispersing the washed magnetite nanoparticles into $HClO_4$ aqueous solution (pH 3) (See scheme 1). At this low pH, the aqueous-suspended IONP become positively charged, due to the protonation of the hydroxylated groups at the surface of the nanoparticle. Eventual aggregates of particles were eliminated by centrifugation (4500 rpm, 10 min). Zeta potential (ξ) and hydrodynamic average diameter (D_H) were assessed using a Malvern Zetasizer instrument (nanoseries Nano Z590), providing ξ = + 46 mV and D_H = 76 nm. A second colloidal sample was prepared by dispersing the as-synthesized magnetite nanoparticles in sodium citrate solution (pH 5.5 adjusted with NaOH), following dialysis against ultrapure water to obtain dispersions with final citrate concentration of 0.05 mol×L^{-1}. For the citrate-functionalized sample (IONP@cit) we found ξ = -47 mV and D_H = 75 nm. The citrate anions adsorbed onto the nanoparticles' surface render them negative charge forming stable colloidal dispersion at pH 7. The high zeta potential values account for the high colloidal stability of the as-prepared suspensions. These two colloidal suspensions were employed as a source of IONP in the assembly of LbL multilayers. TEM was employed to evaluate the morphology of the IONP samples using a JEOL 1011 transmission electron microscope. Scheme 1 exhibits a typical TEM image of the as prepared IONP, that are from the same synthesis process of the investigation published in Letti *et al*. (2017), displaying the same average particle diameter, D_m = 7.4 ± 0.1 nm and standard diameter deviation σ = 0.25 ± 0.01.

2.3 Nanocomposite assembly

The layer-by-layer approach (Decher *et al*. 1992, Decher 1997) has been widely employed as a simple and efficient technique for assembling several types of nanoobjects such as metal particles

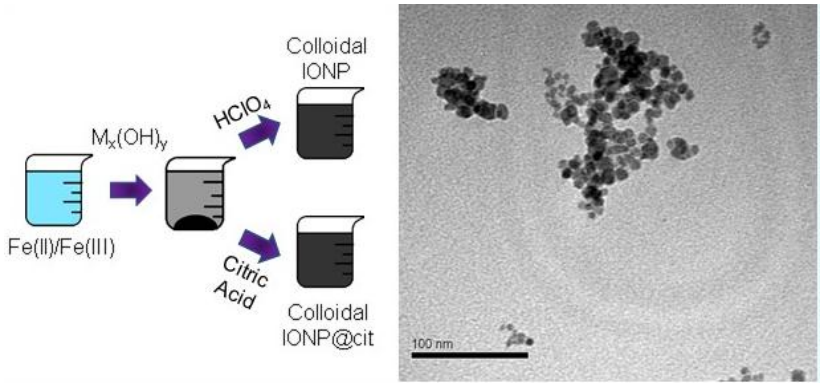

Scheme 1 Schematic representation of IONP synthesis and its dispersion as stable colloids (left panel) and Typical TEM micrograph of IONP (right panel)

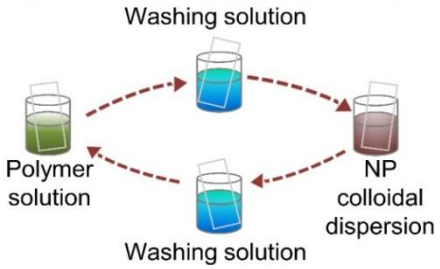

Scheme 2 Illustration of the LbL assembly of IONP/polyelectrolyte nanocomposite

(O'Neal *et al*. 2017), graphene oxide (Nan *et al*. 2016), conjugated polymers (Ferreira and Rubner 1995), polysaccharides (Mattoso *et al*. 1995), proteins (Lvov *et al*. 1995), graphene oxide (Gross *et al*. 2014, Han *et al*. 2016) and oxide nanoparticles (Soler *et al*. 2012b, Paterno and Soler 2013). Importantly, the LbL assembly is conducted at room temperature, from solutions or dispersions previously prepared. In a typical LbL deposition, each component is adsorbed independently (through dipping into solution or by spray) (Seo *et al*. 2016), followed by a rinsing and drying steps to remove the excess of the adsorbed component, as illustrated in Scheme 2. In this approach, the components are maintained attached due to several types of interactions such as electrostatic, H-bonding, covalent bonding, bio-specific recognition, and coordination (Hammond 2004, Ariga *et al*. 2007). Under electrostatic driven LbL, the net charge of the substrate is overcompensated by the upcoming polyelectrolyte layer and thus the initial substrate charge is reversed. When this condition is reached, the process ends and no more additional polyelectrolyte are adsorbed due to inherent electrostatic repulsions. Moreover, the LbL technique is quite inexpensive once it does not require clean rooms and it is conducted at room temperature using common glassware.

In the present report, the as-prepared colloidal suspensions were employed as sources of positively- (IONP) or negatively-charged (IONP@cit) nanoparticles and assembled with anionic polyelectrolyte (sodium sulfonate polystyrene - PSS) or cationic (polyaniline – PANI), respectively. PSS has been chosen because it is a negatively-charged polyelectrolyte and, therefore, suitable for electrostatic LbL assembly with positively-charged IONP. Besides that, PSS is thermally stable up to 450℃, as shown by its thermogravimetric curve (Patrocinio *et al*. 2010).

Moreover, we have been using PSS for LbL film deposition aiming different applications, as for instance electrodes for chemical sensors (Santos *et al*. 2014). Among the hosting conducting polymers, PANI is a conjugated polymer which can be turned conducting or insulating by simple acid–base reactions (Huang *et al*. 1986) and can be successfully LbL assembled with IONP (Paterno *et al*. 2009a).

IONP and IONP@cit aqueous suspensions were prepared directly from dilution of the stock colloidal samples whereas IONP/PSS and PANI/IONP@cit; multilayered nanocomposite films were assembled onto cleaned substrates via the LbL technique as follows (Paterno *et al*. 2010): (i) immersion of the negatively-charged substrates for 3 min into IONP suspension or PANI solution; (ii) substrates were then removed and immersed in a cleaning solution for 20 s (diluted HCl, pH 2.7 or pH 3); (iii) substrates were blow-dried with nitrogen; (iv) substrates were immersed for 3 min into PSS solution or IONP@cit suspension, (pH 3 or pH 7); (v) immersion into the cleaning solution for 20 s, and (vi) blow-drying with nitrogen (see Scheme 2). At the end of these steps each substrate contained a bilayer of IONP/PSS or PANI/IONP@cit, whereas their successive repetition resulted in multilayered films. Multilayered film samples were labeled as $(IONP/PSS)_n$ and $(PANI/IONP@cit)_n$, where n refers to the number of bilayers. It is important to point out here that the term 'bilayer' refers to a pair of cationic/anionic materials and not to a continuous layer of cationic material coated by a continuous layer of anionic material. These films are deposited by successive dipping of the substrate into the cationic and anionic suspensions, but they are not stratified in definite layers as in molecular beam epitaxy or atomic layer deposited films. Therefore, the subscript n in the repeating unit structure, $(IONP/PSS)_n$ or $(PANI/IONP@cit)_n$, refers to the number of deposition cycles. In addition, samples prepared with a single deposition of polymer or IONP were also analyzed by AFM. The interparticle distances within the multilayered film can be finely tuned by varying physicochemical conditions of deposition suspensions as well as by the number of deposited layers (Paterno *et al*. 2009a, Soler *et al*. 2012a, Paterno *et al*. 2012).

2.4 Characterization

Monitoring of adsorbed multilayers onto plain glass substrates was carried out ex situ using UV–vis spectroscopy (Varian Cary 5000). Raman spectra of film $(IONP/PSS)_{10}$ were recorded at room temperature using a commercial Jobin-Yvon triple micro-Raman spectrometer Model T64000 equipped with a liquid-Nitrogen cooled CCD (charge coupled device) detector. The 514 nm line of an Argon ion laser was used to illuminate the sample with intensity of 0.3 mW. AFM images (surface topography) of nanofilms were assessed using a Dimension Icon Bruker system, employing silicon tips attached to a cantilever (spring constant of 40 $N \times m^{-1}$). All images were recorded in the tapping mode while the surface root-mean-square roughness (R_{rms}) was calculated using the software provided by the instrument. Values measured at three different spots on the sample surface were used to calculate the average R_{rms}. TEM cross-section images were recorded with a 200-kV instrument (JEOL JEM 2100). Preparation of the Si substrate-deposited nanocomposite films followed a standard protocol: films were firstly glued face-to-face, then the Si substrate was mechanically ground down to about 20 μm in thickness, following ion milling of the sample to perforation. Electrochemical measurements were performed on $(PANI/IONP@cit)_{20}$ deposited onto Indium-doped tin oxide (ITO) substrates. The film deposition was limited to a geometric active area of 0.36 cm^2 on the substrate. The electrochemical behavior of these samples as the working electrode was investigated by cyclic voltammetry and chronopotentiometry in a three-electrode configuration cell (reference electrode: Ag/AgCl; counter electrode: Pt) in 0.5

mol×L^{-1} Na_2SO_4 as the electrolyte solution). Both experiments were carried out with a Metrohm Autolab PGSTAT 204 potentiostat, at room temperature (25℃) and after purging the electrochemical cell with N_2 for 20 min.

3. Results and discussion

3.1 Nanocomposite assembly monitoring and properties

Usually, monitoring of the IONP/polyelectrolyte LbL assembly onto glass slides is carried out by UV-vis spectroscopy. Despite its simplicity and easy handling, UV-vis spectroscopy presents some limitation when applied to detect iron oxide materials in the sub-microgram range whereas the quartz crystal microbalance (QCM) technique coupled to a flow injection system can precisely monitor the uptake of IONP and polyelectrolyte during LbL deposition (Alcantara *et al*. 2011a). Figs. 1(a)-(b) display UV-vis spectra of $(IONP/PSS)_n$ and $(PANI/IONP@cit)_n$ nanocomposites, respectively, comprising different number of bilayers, from n = 2 up to n = 10 bilayers. In Fig. 1(a) it is observed a shoulder at 480 nm characteristic of magnetite and attributed to the $Fe^{2+} \rightarrow Fe^{3+}$ electron transfer process (Schwertmann and Cornell 1991) whereas PSS does not show any absorption in the visible range. It is observed a shoulder at 440 nm in Fig. 1(b) relative to magnetite, as well as a broad band whose peak is centered at 640 nm attributed to PANI. A stepwise film growth is observed in the inset of both Figs. 1(a)-(b), in which the amount of IONP increases almost linearly with the number of bilayers, the same occurring for PANI (see Fig. 1(b)). This behavior indicates that equal amounts of each material are adsorbed per bilayer. Thus, the LbL process provides a fine control of nanocomposites composition by simply varying the number of nanoparticle/polyelectrolyte bilayers. Similar results are observed with other nanoparticle/ polyelectrolyte systems when adsorption is driven by electrostatic attraction (Alcantara *et al*. 2011b).

The surface morphology of nanocomposite films was inspected by tapping-mode AFM. In this mode, the sample is scanned by an oscillating tip probe whose oscillation amplitude is sensitive to both topography and mechanical properties of the sample's surface. Topography and phase AFM

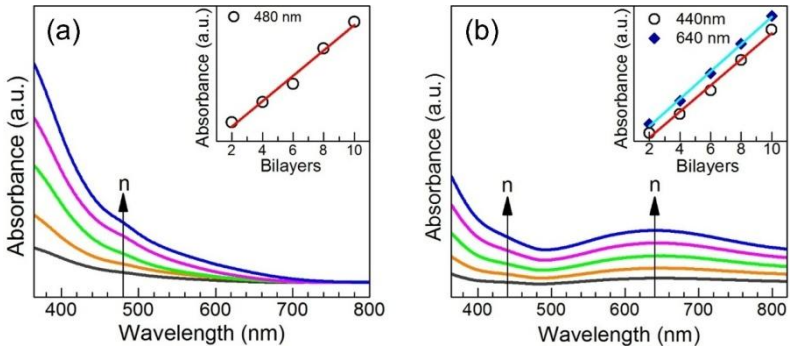

Fig. 1 Monitoring of nanocomposites deposition by UV-vis spectroscopy. (a) $(IONP/PSS)_n$, reprinted with permission from Letti *et al*. (2017) © 2017, Elsevier B.V.; and (b) $(PANI/IONP@cit)_n$; n = 2, 4, 6, 8, and 10 bilayers. Insets show increment of nanocomposites absorption as a function of deposited bilayers. Straight lines are drawn only as guide to the eyes

images displayed in Figs. 2(a)-(f) show the surface morphology monitoring at the first adsorbed monolayers, polymer ((a)-(b)) and IONP ((c)-(d)), respectively, and $(IONP/PSS)_{9.5}$ and nanocomposite ((e)-(f)). Image displayed in Fig. 2(a) shows the presence of small globules which arise from typical nucleated adsorption process, as already observed for similar polymer systems (Paterno and Mattoso 2001, Leite *et al*. 2005), in agreement with the phase image shown in Fig. 2(b).

AFM topography image presented in Fig. 2(c) shows spherical structures arranged as a densely-packed layer and distributed over the entire substrate, thus confirming the presence of IONP. AFM topography image collected from the $(IONP/PSS)_{9.5}$ nanocomposite (Fig. 2(e)), in which IONP is the top layer, shows a larger number of agglomerates when compared with the nanoparticle monolayer (Fig. 2(c)). In these samples, structures in phase images (Fig. 2(d)-(f)) match with the features presented in their respective topography images (Fig. 2(c)-(e)). The surface roughness (root-mean square; R_{rms}) of the first monolayer IONP, $(IONP/PSS)_5$ and $(IONP/PSS)_{9.5}$ samples determined by AFM were found to be 8, 12 and 13 nm, respectively. The R_{rms} value for the first monolayer corresponds roughly to the nanoparticle diameter, whereas close values of surface roughness for nanocomposites with 5 and 9.5 bilayers were found, indicating uniform surface morphology as the number of bilayers increases.

The surface morphology of the $(PANI/IONP@cit)_{10}$ nanocomposite was assessed by scanning electron microscopy. As a conducting polymer, the nanocomposite sample comprising PANI could be analyzed as prepared. SEM image presented in Fig. 3(a) evidences the uniformity of the surface morphology, showing no regions composed by only particles separated from polymer, with no phase segregation of nanoparticles and polymer. Fig. 3(b) displays the cross-sectional high

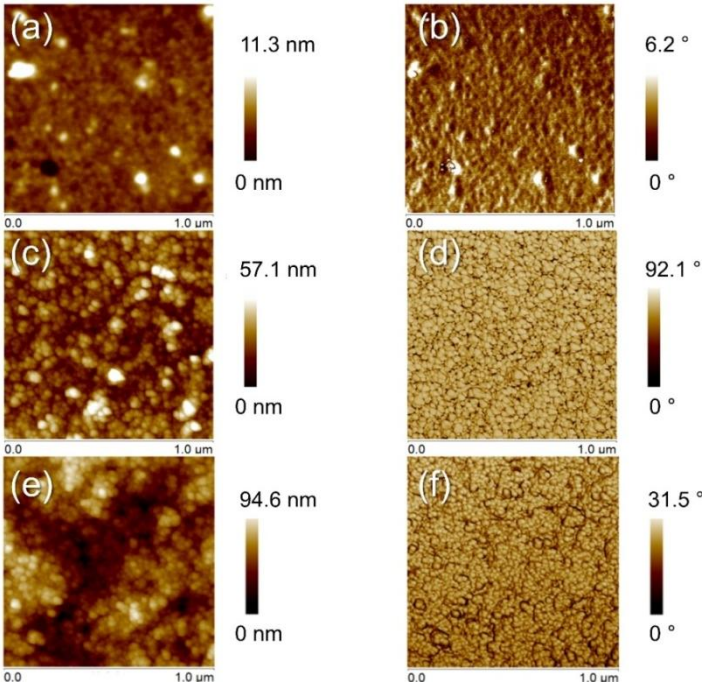

Fig. 2 Topography ((a)-(c)-(e)) and phase ((b)-(d)-(f)) AFM images of: the first LbL monolayer of polymer ((a)-(b)); the first LbL monolayer of IONP adsorbed ((c)-(d)); $(IONP/PSS)_{9.5}$ nanocomposite ((e)-(f))

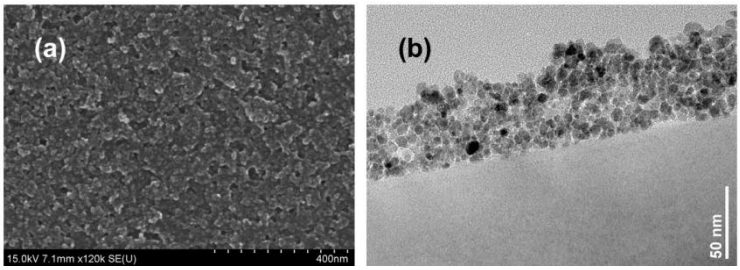

Fig. 3 SEM (a); and HRTEM Cross-sectional (b) images for $(PANI/IONP@cit)_{10}$

resolution transmission electron microscopy (HRTEM) micrograph of $(PANI/IONP@cit)_{10}$. It is observed that IONP nanocrystals are distributed homogeneously throughout the nanocomposite whereas dressed by a tinny layer of PANI (brighter layer), thus keeping nanocrystals isolated from each other. Further, the distance between particles of about 2.5 nm was estimated from HRTEM images and confirmed by the value obtained from simulated pair distribution function (Neumann *et al*. 2013). The evidence of nanoparticle wrapped by polymer chains was confirmed by electrical measurements (Alcantara *et al*. 2013b).

3.2 Investigation of the effect of thermal annealing

Raman spectroscopy has been intensively employed to investigate structural features of IONP as colloidal suspensions or solid samples (Morais *et al*. 2000, Chourpa *et al*. 2005, Melo *et al*. 2006, Ayyappan *et al*. 2010). Also, the oxidation process of nanocrystalline magnetite films has been successfully studied through Raman spectroscopy (Bourgeois *et al*. 2013, Park 2009, Trudel *et al*. 2011, Letti *et al*. 2017). The iron oxide phase finger print nanocomposites can be unequivo-

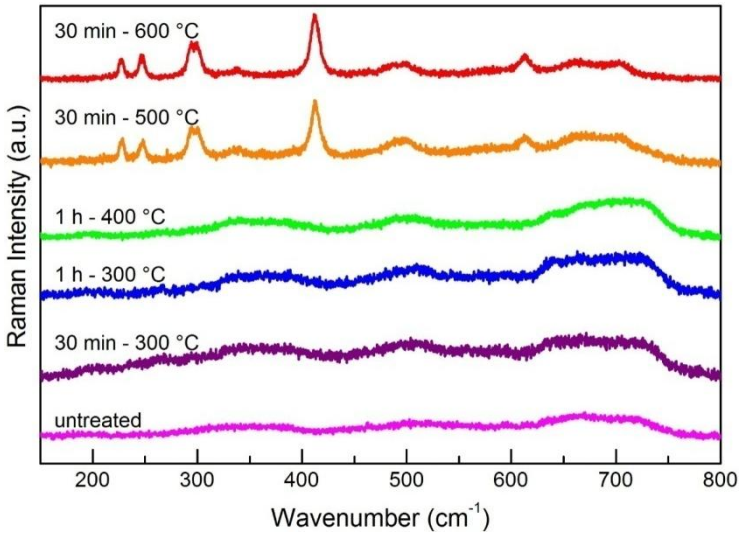

Fig. 4 Raman spectra of $(IONP/PSS)_{10}$ nanocomposite sample registered with laser (λ = 514 nm) intensity of 0.3 mW, before and after performing different thermal annealing in air atmosphere, as indicated

cally probed by Raman spectroscopy (Paterno *et al*. 2012, Letti *et al*. 2017). Aiming to study the oxidation process of IONP embedded into the nanocomposites as a function of thermal treatments, we have carried out a study in which the effect of heating samples in an oxidative atmosphere was ex situ monitored. Briefly, the $(IONP/PSS)_{10}$ nanocomposite sample was air annealed at different temperatures (from 300℃ to 600℃), as indicated in Fig. 4, namely for 30 min at 300℃, for 1 h at 300℃, for 1 h at 400℃, for 30 min at 500℃, and for 30 min at 600℃. Raman spectrum was recorded after each annealing step, keeping the laser intensity as low as 0.3 mW in order to avoid additional sample annealing (da Silva *et al*. 2003). Fig. 4 shows the Raman spectrum for each thermal annealing investigated. It is observed that the Raman spectrum of the untreated $(IONP/PSS)_{10}$ sample corresponds to the oxidized magnetite with broad bands peaking at 350, 500, and 700 cm^{-1} characteristics of maghemite (Soler and Fanyao 2012). Further, for samples annealed at temperatures lower than 400℃ we observed Raman spectra corresponding to the maghemite phase. Only at 500℃ the characteristic Raman peaks of the hematite phase at 217, 228, 294 and 391 cm^{-1} were observed. This is because at 500℃ PSS starts degrading, in accordance with the reported TG curve (Patrocinio *et al*. 2010). These findings indicate that PSS protects maghemite IONP LbL assembled from oxidation/phase transformation to hematite, maintaining the magnetic characteristics of the nanocomposites. Only after PSS degradation the hematite phase arises.

3.3 Applications

Nanostructured materials based on LbL films of IONP and PANI have been developed and tested as electrodes for supercapacitors. The electrochemical behavior of $(PANI/IONP@cit)_{20}$ nanocomposite films as the working electrode was investigated by cyclic voltammetry and chronopotentiometry in a three-electrode configuration cell (reference electrode: Ag/AgCl; counter electrode: Pt) in 0.5 mol×L^{-1} Na_2SO_4 as the electrolyte solution. Fig. 5 shows the cyclic voltammograms of the as-prepared $(PANI/IONP@cit)_{20}$ nanocomposite films registered in Na_2SO_4 0.5 mol×L^{-1}, pH = 6. This electrolyte medium was chosen since more acidic pHs can degrade PANI after successive charge-discharge cycles. It also avoids eventual dissolution of the

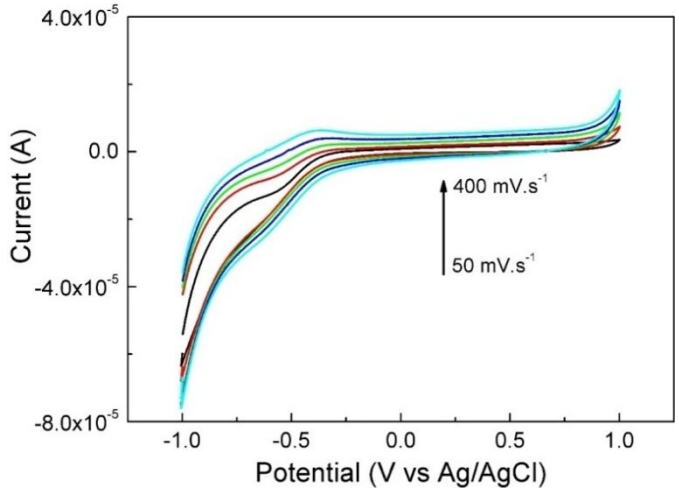

Fig. 5 Cyclic voltammograms of $(PANI/IONP@cit)_{20}$ modified ITO electrode at different scan rates, as indicated. Electrolyte: 0.5 mol×L^{-1} Na_2SO_4. Electrode active area: 0.36 cm^2

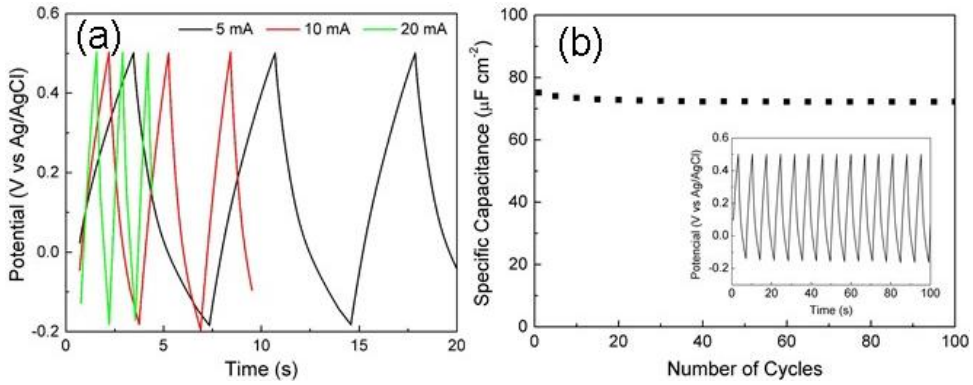

Fig. 6 Electrochemical performance of $(PANI/IONP@cit)_{20}$ modified ITO electrode. (a) Galvanostatic charge-discharge curves acquired at different applied currents, as indicated and (b) specific capacitance versus number of charge-discharge cycles at 5 μA of applied current. The inset shows the first fourteen charge-discharge cycles. Electrolyte: 0.5 mol×L^{-1} Na_2SO_4. Electrode active area: 0.36 cm^2

IONP@cit. In the range between +1.0 V and 0 V, no electrochemical reaction is detected despite the discreet enlargement of the voltammograms as the potential scan rate is increased. In this range, PANI shows two reversible redox reactions under acidic pH electrolyte medium (Huang *et al*. 1986). Therefore, none of these reactions should be expected under this working condition. In the potential range right below 0 V to -1.0 V, the voltammogram is enlarged and shows a pair of subtle peaks that are ascribed to the interconversion between maghemite and magnetite phases, or else γ-$Fe_2O_3 \leftrightarrow Fe_3O_4$. The respective cathodic/anodic potentials are [-0.625 V/-390 V], which are negatively shifted in comparison to the behavior investigated while in acetate buffer, pH = 4.6 (Santos *et al*. 2014). The enlarged voltammogram in this range suggests the potential use of the $(PANI/IONP@cit)_{20}$ nanocomposite films as electrodes for supercapacitors.

Fig. 6 displays the galvanostatic charge-discharge curves acquired at different charging currents (Fig. 6(a)) and the variation of the specific capacitance with successive charge-discharge cycles (Fig. 6(b)). As expected, Fig. 6(a) shows that the charging time is faster for higher charging currents. The specific capacitance (Csp) was determined from the galvanostatic curves based on the following equation: $Csp = I \times \Delta t/AV$, where I is the charge current (in amperes), Δt is the elapsed time for charge discharge (in seconds), A is the active area (in cm^2) and V the potential (vs Ag/AgCl, in volts). Up to 100 hundred charge-discharge cycles, the specific capacitance remains almost constant in 72.6 ± 0.5 $\mu F \times cm^{-2}$, as seen in Fig. 6(b). This value can even be improved with the deposition of more (PANI/IONP@cit) bilayers. The first fourteen charge-discharge cycles are provided in the inset, which shows the reversible response of the $(PANI/IONP@cit)_{20}$ based capacitor. In summary, the layer-by-layer $(PANI/IONP@cit)_n$ nanocomposite films represent a very promising direction for the development of low cost supercapacitors.

4. Conclusions

In the present report, IONP were successfully assembled with PSS or PANI, comprising two systems based on electrostatic interactions, in which the adsorption process is highly regulated and

thus nanocomposite composition and structure were fine tailored. The internal structure of the resulting nanocomposites features individual nanoparticles enclosed by an extremely thin layer of polyelectrolytes, as shown by cross-sectional TEM images and confirmed by electrical measurements.

The $(IONP/PSS)_{10}$ nanocomposite sample was annealed at different temperatures, from 300℃ to 600℃. After each annealing step, Raman spectra were recorded. Our findings indicate that for temperatures lower than 400℃, PSS protects maghemite-based IONP LbL assembled from oxidation/phase transformation to hematite, maintaining the magnetic characteristics of the nanocomposites.

Layer-by-layer $(PANI/IONP@cit)_{20}$ nanocomposite film, assembled onto Indium-doped tin oxide (ITO) substrates, was investigated by cyclic voltammetry and chronopotentiometry, aiming to probe its electrochemical behavior as working electrode. Our findings suggest the potential use of these $(PANI/IONP@cit)_{20}$ nanocomposite films as electrodes for the development of low cost supercapacitors.

Acknowledgments

Maria A.G. Soler thanks Professor Steve Granick University of Illinois at Urbana-Champaign, United States, and CAPES-Brazil (4410-08-4), to provide access to the Frederick Seitz Material Research Laboratory facilities. We are grateful to Dr. J.G. Wen (Electron Microscopy Center, Materials Science Division, Argonne National Laboratory, Argonne, Illinois, United States) for the support in the TEM measurements. Leonardo G. Paterno thanks to financial support of Brazilian agencies FAP-DF (0193, 000829/2015) and FINEP (01/13/0470/00). In addition, financial support of Brazilian agencies MCT-CNPq, CAPES, and FAP-DF, is gratefully acknowledged.

References

Alcantara, G.B., Paterno, L.G., Afonso, A.S., Faria, R.C., Pereira-da-Silva, M.A., Morais, P.C. and Soler, M.A.G. (2011a), "Adsorption of cobalt ferrite nanoparticles within layer-by-layer films: a kinetic study carried out using quartz crystal microbalance", *Phys. Chem. Chem. Phys.*, **13**(48), 21233-21242.

Alcantara, G.B., Paterno, L.G., Fonseca, F.J., Morais, P.C. and Soler, M.A.G. (2011b), "Morphology of cobalt ferrite nanoparticle–polyelectrolyte multilayered nanocomposites", *J. Magn. Magn. Mater.*, **323**(10), 1372-1377.

Alcantara, G.B., Paterno, L.G., Fonseca, F.J., Pereira-da-Silva, M.A., Morais, P.C. and Soler, M.A.G. (2013a), "Dielectric properties of cobalt ferrite nanoparticles in ultrathin nanocomposite films", *Phys. Chem. Chem. Phys.*, **15**(45), 19853-19861.

Alcantara, G.B., Paterno, L.G., Fonseca, F.J., Pereira-da-Silva, M.A., Morais, P.C. and Soler, M.A.G. (2013b), "Layer-by-layer assembled cobalt ferrite nanoparticles for chemical sensing", *J. Nanofluids*, **2**(3), 175-183.

Alivisatos, A.P. (1996), "Semiconductor clusters, nanocrystals, and quantum dots", *Science*, **271**, 933-937.

Ariga, K., Hill, J.P. and Ji, Q. (2007), "Layer-by-layer assembly as a versatile bottom-up nanofabrication technique for exploratory research and realistic application", *Phys. Chem. Chem. Phys.*, **9**(19), 2319-2340.

Aroutiounian,V.M, Arakelyan, V.M., Shahnazaryan, G.E., Aleksanyan, M.S., Hernadi, K., Nemeth, Z., Berki, P., Papa, Z., Toth, Z. and Forro, L. (2015), "The ethanol sensors made from α-Fe_2O_3 decorated with multiwall carbon nanotubes", *Adv. Nano Res., Int. J.*, **3**(1), 1-11.

Ayyappan, S., Mahadevan, S., Chandramohan, P., Srinivasan, M.P., Philip, J. and Raj, B. (2010), "Influence of Co2+ ion concentration on the size, magnetic properties, and purity of $CoFe_2O_4$ spinel ferrite

nanoparticles", *J. Phys. Chem.* C, **114**(14), 6334-6341.
Balazs, A.C., Emrick, T. and Russel, T.P. (2006), "NNanoparticle polymer composites: Where two small worlds meet", *Science*, **314**(5802), 1107-1110.
Begin-Colin, S. and Felder-Flesch, D. (2012), "Functionalizsation of Magnetic Iron Oxide Nanoparticles", In: *Magnetic Nanoparticles from Fabrication to Clinical Applications*, (N.T.K. Thank Ed.), CRC Press Taylor & Francis Group, Boca Raton, FL, USA, pp. 151-191.
Blums, E., Cebers, A. and Maiorov, M.M. (1985), *Magnetic Fluids*, Walter de Gruyter, Berlin, Germany.
Bourgeois, F., Gergaud, P., Renevier, H., Leclere, C. and Feuillet, G. (2013), "Low temperature oxidation mechanisms of nanocrystalline magnetite thin film", *J. Appl. Phys.*, **113**(1), 013510.
Bruchez, M. Jr., Moronne, M., Gin, P., Weiss, S. and Alivisatos, A.P. (1998), "Semiconductor nanocrystals as fluorescent biological labels", *Science*, **281**(5385), 2013-2016.
Butt, F.A. and Jafri, S.M.M. (2015), "Effect of nucleating agents and stabilisers on the synthesis of Iron-Oxide Nanoparticles-XRD analysis", *Adv. Nano Res., Int. J.*, **3**(3), 169-176
Chen, Y.P., Zou, M., Qi, C., Xie, M.-X., Wang, D.-N., Wang, Y.-F., Xue, Q., Li, J.-F. and Chen, Y. (2013), "Immunosensor based on magnetic relaxation switch and biotin–streptavidin system for the detection of kanamycin in milk", *Biosens. Bioelectron.*, **39**(1), 112-117.
Chourpa, I., Douziech-Eyrolles, L., Ngaboni-Okassa, L., Fouquenet, J.-F., Cohen-Jonathan, S., Soucé, M., Marchais, H. and Dubois, P. (2005), "Molecular composition of iron oxide nanoparticles, precursors for magnetic drug targeting, as characterized by confocal Raman microspectroscopy", *Analyst*, **130**(10), 1395-1403.
Correa-Duarte, M.A., Giersig, M., Kotov, N.A. and Liz-Marzán, L.M. (1998), "Control of Packing Order of Self-Assembled Monolayers of Magnetite Nanoparticles with and without SiO_2 Coating by Microwave Irradiation", *Langmuir*, **14**(22), 6430-6435.
da Silva, S.W., Melo, T., Soler, M.A.G., Da Silva, M.F., Lima, E.C.D. and Morais, P.C. (2003), "Stability of citrate-coated magnetite and cobalt-ferrite nanoparticles under laser irradiation: a Raman spectroscopy investigation", *IEEE Trans. Magn.*, **39**(5), 2645-2647.
Dalpozzo, R. (2015), "Magnetic nanoparticle supports for asymmetric catalysts", *Green Chem.*, **17**(7), 3671-3686.
Decher, G. (1997), "Fuzzy nanoassemblies: toward layered polymeric multicomposites", *Science*, **277**(5330), 1232-1237.
Decher, G., Hong, J.D. and Schmitt, J. (1992), "Buildup of ultrathin multilayer films by a self-assembly process: III. Consecutively alternating adsorption of anionic and cationic polyelectrolytes on charged surfaces", *Thin Sol. Films*, **210**, 831-835.
Dey, S., Mohanta, K. and Pal, A.J. (2010), "Magnetic-field-assisted layer-by-layer electrostatic assembly of ferromagnetic nanoparticles", *Langmuir*, **26**(12), 9627-9631.
Ferreira, M. and Rubner, M.F. (1995), "Molecular-level processing of conjugated polymers. 1. Layer-by-layer manipulation of conjugated polyons", *Macromolecules*, **28**(21), 7107-7114.
Gao, Z., Ma, T., Zhao, E., Docter, D., Yang, W., Stauber, R.H. and Gao, M. (2016), "Small is smarter: nano MRI contrast agents–advantages and recent achievements", *Small*, **12**(5), 556-576.
Grassian, V.H. (2008), "When size really matters: size-dependent properties and surface chemistry of metal and metal oxide nanoparticles in gas and liquid phase environments", *J. Phys. Chem. C*, **112**(47), 18303-18213.
Grigoriev, D., Gorin, D. Sukhorukov, G.B., Yashchenok, A., Maltseva, E. and Möhwald, H. (2007), "Polyelectrolyte/magnetite nanoparticle multilayers: Preparation and structure characterization", *Langmuir*, **23**(24), 12388-12396.
Gross, M.A., Sales, M.J.A., Soler, M.A.G., Pereira-da-Silva, M.A., da Silva, M.F.P. and Paterno, L.G. (2014), "Reduced graphene oxide multilayers for gas and liquid phases chemical sensing", *RSC Adv.*, **4**(34), 17917-17924.
Hammond, P.T. (2004), "Form and function in multilayer assembly: New applications at the nanoscale", *Adv. Mater.*, **16**(15), 1271-1293.
Han, U., Seo, Y. and Hong, J. (2016), "Effect of pH on the structure and drug release profiles of layer-by-

layer assembled films containing polyelectrolyte, micelles, and graphene oxide", *Sci. Rep.*, **6**, 24158.
Ho, D., Sun, X. and Sun, S. (2011), "Monodisperse magnetic nanoparticles for theranostic applications", *Acc. Chem. Res.*, **44**(10), 875-882.
Huang, W.-S., Humphrey, B.D. and MacDiarmid, A.G. (1986), "Polyaniline, a novel conducting polymer. Morphology and chemistry of its oxidation and reduction in aqueous electrolytes", *J. Chem. Soc. Faraday Trans.*, 1, **82**(8), 2385-2400.
Jolivet, J.-P., Cassaignon, S., Chanéac, C., Chiche, D., Durupthy, O. and Portehault, D. (2010), "Design of metal oxide nanoparticles: control of size, shape, crystalline structure and functionalization by aqueous chemistry", *Compte-Rendu de Chimie de l'Académie des Sciences*, **13**(1), 40-51.
Kang, Y.S., Risbud, S., Rabolt, J.F. and Stroeve, P. (1996), "Synthesis and characterization of nanometer-size Fe_3O_4 and γ-Fe_2O_3 particles", *Chem. Mater.*, **8**(9), 2209-2211.
Kim, H.S., Sohn, B.H., Lee, W., Lee, J.-K., Choi, S.J. and Kwon, S.J. (2002), "Multifunctional layer-by-layer self-assembly of conducting polymers and magnetic nanoparticles", *Thin Solid Films*, **419**(1), 173-177.
Ko, Y., Shin, D., Koo, B., Lee, S.W., Yoon, W.S. and Cho, J. (2015), "Ultrathin supercapacitor electrodes with high volumetric capacitance and stability using direct covalent-bonding between pseudocapacitive nanoparticles and conducting materials", *Nano Energy*, **12**, 612-625.
Kurtinaitienė, M., Mažeika, K., Ramanavičius, S., Pakštas, V. and Jagminas, A. (2016), "Effect of additives on the hydrothermal synthesis of manganese ferrite nanoparticles", *Adv. Nano Res., Int. J.*, **4**(1), 1-14.
Leite, F.L., Paterno, L.G., Borato, C.E., Herrmann, P.S.P, Oliveira, O.N. and Mattoso, L.H.C. (2005), "Study on the adsorption of poly (o-ethoxyaniline) nanostructured films using atomic force microscopy", *Polymer*, **46**(26), 12503-12510.
Letti, C.J., Paterno, L.G., Pereira-da-Silva, M.A., Morais, P.C. and Soler, M.A.G. (2017), "The role of polymer films on the oxidation of magnetite nanoparticles", *J. Solid. State. Chem.*, **246**, 57-64.
Lvov, Y.K., Ariga, I., Ichinose, I. and Kunitake, T. (1995), "Assembly of multicomponent protein films by means of electrostatic layer-by-layer adsorption", *J. Am. Chem. Soc.*, **117**(22), 6117-6123.
Magnani, M., Galluzzi, L. and Bruce, I.J. (2006), "The use of magnetic nanoparticles in the development of new molecular detection systems", *J. Nanosc. Nanotech.*, **6**(8), 1-10.
Mamedov, A. Ostrander, J., Aliev, F. and Kotov, N.A. (2000), "Stratified assemblies of magnetite nanoparticles and montmorillonite prepared by the layer-by-layer assembly", *Langmuir*, **16**(8), 3941-3949.
Marinică, O., Susan-Resiga, D., Bălănean, F., Vizman, D., Socoliuc, V. and Vékás, L. (2016), "Nano-micro composite magnetic fluids: Magnetic and magnetorheological evaluation for rotating seal and vibration damper applications", *J. Magn. Magn. Mater.*, **406**, 134-143.
Massart, R., Dubois, E., Cabuil, V. and Hasmonay, E. (1995), "Preparation and properties of monodisperse magnetic fluids", *J. Magn. Magn. Mater.*, **149**(1-2), 1-5.
Mattoso, L.H.C., Zucolotto, V., Paterno, L.G., van Griethuijsen, R., Ferreira, M., Campana, S.P. and Oliveira, Jr. O.N. (1995), "Self-assembly films of polyacids and doped poly (o-alkoxyanilines)", *Synth. Met.*, **71**(1-3), 2037- 2038.
Melo, T.F.O., da Silva, S.W., Soler, M.A.G., Lima, E.C.D. and Morais, P.C. (2006), "Investigation of surface passivation process on magnetic nanoparticles by Raman spectroscopy", *Surf. Sci.*, **600**(18), 3642-3645.
Morais, P.C, da Silva, S.W., Soler, M.A.G. and Buske, N. (2000), "Raman investigation of uncoated and coated magnetic fluids", *J. Phys. Chem. A*, **104**(13), 2894-2896.
Nan, Q., Li, P. and Cao, B. (2016), "Fabrication of positively charged nanofiltration membrane via the layer-by-layer assembly of graphene oxide and polyethylenimine for desalination", *Appl. Surf. Sci.*, **387**, 521-528.
Neumann, R.F., Bahiana, M., Paterno, L.G., Soler, M.A.G., Sinnecker, J.P, Wen, J.G. and Morais, P.C. (2013), "Morphology and magnetism of multifunctional nanostructured γ-Fe_2O_3 films: Simulation and experiments", *J. Magn. Magn. Mater.*, **347**, 26-32.
O'Neal, J.T., Bolen, M.J., Dai, E.Y. and Lutkenhaus, J.L. (2017), "Hydrogen-bonded polymer nanocomposites containing discrete layers of gold nanoparticles", *J. Colloid Interf. Sci.*, **485**, 260-268.

Paterno, L.G. and Mattoso, L.H.C. (2001), "Effect of pH on the preparation of self-assembled films of poly (o-ethoxyaniline) and sulfonated lignin", *Polymer*, **42**(12), 5239-5245.

Paterno, L.G. and Soler, M.A.G. (2013), "Layer-by-layer enabled nanomaterials for chemical sensing and energy conversion", *Jom*, **65**(6), 709-719.

Paterno, L.G., Soler, M.A.G., Fonseca, F.J., Sinnecker, J.P., Sinnecker, E.H.C.P., Lima, E.C.D., Novak, M.A. and Morais, P.C. (2009a), "Layer-by-layer assembly of bifunctional nanofilms: Surface-functionalized maghemite hosted in polyaniline", *J. Phys. Chem.* C, **113**(13), 5087-5095.

Paterno, L.G., Alcantara, G.B., Fonseca, F.J., Soler, M.A.G., Sinnecker, J.P., Novak, M.A., Lima, E.C.D. and Morais, P.C. (2009b), "Fabrication and characterization of nanostructured conducting polymer films containing magnetic nanoparticles", *Thin Solid Films*, **517**(5), 1753-1758.

Paterno, L.G., Soler, M.A.G., Fonseca, F.J., Sinnecker, J.P., Sinnecker, E.H.C.P., Lima, E.C.D., Bao, S.N., Novak, M.A. and Morais, P.C. (2010), "Magnetic nanocomposites fabricated via the layer-by-layer approach", *J. Nanosci. Nanotech.*, **10**(4), 2679-2685.

Paterno, L.G, Sinnecker, E.H.C.P., Soler, M.A.G., Sinnecker, J.P., Novak, M.A. and Morais, P.C. (2012), "Tuning of magnetic dipolar interactions of maghemite nanoparticles embedded in polyelectrolyte layer-by-layer films", *J. Nanosci. Nanotechnol.*, **12**(8), 6672-6678.

Patrocinio, A.O.T., Paterno, L.G. and Ilha, N.Y.M. (2010), "Role of polyelectrolyte for layer-by-layer compact TiO2 films in efficiency enhanced dye-sensitized solar cells", *J. Phys. Chem. C*, **114**(41), 17954-17959.

Park, S. (2009), "Preparation of iron oxides using ammonium iron citrate precursor: Thin films and nanoparticles", *J. Solid. State. Chem.*, **182**(9), 2456-2460.

Pereira, A., Alves, S., Casanova, M., Zucolotto, V. and Bechtold, I.H. (2010), "The use of colloidal ferrofluid as building blocks for nanostructured layer-by-layer films fabrication", *J. Nanopart. Res.*, **12**(8), 2779-2785.

Philip, J. and Laskar, J.M. (2012), "Optical properties and applications of ferrofluids—A review", *J. Nanofluids*, **1**(1), 3-20.

Pichon, B.P., Louet, P., Felix, O., Drillon, M., Begin-Colin, S. and Decher, G. (2011), "Magnetotunable hybrid films of stratified iron oxide nanoparticles assembled by the layer-by-layer technique", *Chem. Mater.*, **231**(16), 3668-3675.

Qu, F. and Morais, P.C. (2000), "An oxide semiconductor nanoparticle in an aqueous medium: A surface charge density investigation", *J. Phys. Chem. B*, **104**(22), 5232-5236.

Santos, J.G., Souza, J.R., Letti, C.J., Soler, M.A.G., Morais, P.C., Pereira-da-Silva, M.A. and Paterno, L.G. (2014), "Iron oxide nanostructured electrodes for detection of copper (II) ions", *J. Nanosci. Nanotechnol.*, **14**(9), 6614-6623.

Schwertmann, U. and Cornell, R.M. (1991), *Iron Oxides in the Laboratory*: *Preparation and Characterization*, VCH Publishers, New York, NY, USA.

Seo, S., Lee, S. and Park, Y.P. (2016), "Automatic layer-by-layer spraying system for functional thin film coatings", *Rev. Sci. Instrum.*, **87**(3), 036110.

Soler, M.A.G. and Fanyao, Q. (2012), "Raman Spectroscopy of Iron Oxide Nanoparticles", In: *Raman Spectroscopy for Nanomaterials Characterization*, Springer-Verlag, Berlin, Germany, pp. 379-417.

Soler, M.A.G. and Paterno, L.G. (2017), "Magnetic Nanoparticles", In: *Nanostructures*, (O.N. Oliveira, Jr., M. Ferreira, A.L. Da Róz and F.L. Leite), Elsevier, pp. 147-186.

Soler, M.A.G., Silva, S.W., Garg, V.K, Oliveira, A.C., Azevedo, R.B., Pimenta, A.C.M., Lima, E.C.D. and Morais, P.C. (2005), "Surface passivation and characterization of cobalt–ferrite nanoparticles", *Surf. Sci.*, **575**(1), 12-16.

Soler, M.A.G., Lima, E.C.D., Silva, S.W., Melo, T.F.O., Pimenta, A.C.M., Sinnecker, J.P., Azevedo, R.B., Garg, V.K. Oliveira, A.C., Novak, M.A. and Morais, P.C. (2007), "Aging investigation of cobalt ferrite nanoparticles in low pH magnetic fluid", *Langmuir*, **23**(19), 9611-9617.

Soler, M.A.G., Lima, E.C.D., Nunes, E.S., Silva, F.L.R., Oliveira, A.C., Azevedo, R.B. and Morais, P.C. (2011), "Spectroscopic study of maghemite nanoparticles surface-grafted with DMSA", *J. Phys. Chem.* A, **115**(6), 1003-1008.

Soler, M.A.G., Paterno, L.G., Sinnecker, J.P., Wen, J.G., Sinnecker, E.H.C.P., Neumann, R.F., Bahiana, M., Novak, M.A. and Morais, P.C. (2012a), "Assembly of γ-Fe_2O_3/polyaniline nanofilms with tuned dipolar interaction", *J. Nanopart. Res.*, **14**(3), 653.

Soler, M.A., Paterno, L.G. and Morais, P.C. (2012b), "Layer-by-layer assembly of magnetic nanostructures", *J. Nanofluids*, **1**(2), 101-119.

Suda, M., Miyazaki, Y., Hagiwara, Y., Sato, O., Shiratori, S. and Einaga, Y. (2005), "Photoswitchable magnetic layer-by-layer films consisting of azobenzene derivatives and iron oxide nanoparticles", *Chem. Lett.*, **34**(7), 1028-1029.

Sun, Z., Du, J., Yan, L., Chen, S., Yang, Z. and Jing, C. (2016), "Multifunctional Fe3O4@SiO2− Au satellite structured SERS probe for charge selective detection of food dyes", *ACS Appl. Mater. Interfaces*, **8**(5), 3056-3062.

Thuy, T.T. (2012), *Next Generation Magnetic Nanoparticles for Biomedical Applications*. *Magnetic Nanoparticles from Fabrication to Clinical Applications*, (Edited by N.T.K. Thanh), Taylor & Francis Group, Boca Raton, FL, USA.

Toulemon, D., Rastei, M.V., Schmool, D., Garitaonandia, J.S., Lezama, L., Cattoën, X., Bégin-Colin, S. and Pichon, B.P. (2016), "Enhanced collective magnetic properties induced by the controlled assembly of iron oxide nanoparticles in chains", *Adv. Funct. Mater.*, **26**(15), 2454-2462.

Trahms, L. (2010), "Biomedical Applications of Magnetic Nanoparticles", In: *Colloidal Mangetic Fluids*, (S. Odenbach Ed.), Verlag, Berlim Weidelberg, pp. 328-358.

Trudel, S., Crozier, E.D., Gordon, R.A., Budnik, P.S. and Hill, R.H. (2011), "X-ray absorption fine structure study of amorphous metal oxide thin films prepared by photochemical metalorganic deposition", *J. Solid. State. Chem.*, **184**(5), 1025-1035.

Viali, W.R., Alcantara, G.B., Sartoratto, P.P.C., Soler, M.A.G., Mosiniewicz-Szablewska, E., Andrzejewski, B. and Morais, P.C. (2010), "Investigation of the molecular surface coating on the stability of insulating magnetic oils", *J. Phys. Chem.* C, **114**(1), 179-188.

Xiang, Q., Teixeira, C.B., Sun, L. and Morais, P.C. (2016), "Magnetic nanoparticle film reconstruction modulated by immersion within DMSA aqueous solution", *Sci. Rep.*, **6**, 18202.

Yiu, H.H.P., McBain, S.C., Lethbridge, Z.A.D., Lees, M.R. and Dobson, J. (2010), "Preparation and characterization of polyethylenimine-coated Fe_3O_4-MCM-48 nanocomposite particles as a novel agent for magnet-assisted transfection", *J. Biomed. Mater. Res. A*, **92**(1), 386-392.

Wang, Y., Ma, H., Wang, X., Pang, X., Wu, D., Du, B. and Wei, Q. (2015), "Novel Signal Amplification Strategy for Ultrasensitive Sandwich-Type Electrochemical Immunosensor Employing Pd–Fe_3O_4-GS as the Matrix and SiO_2 as the Label", *Biosens. Bioelectron.*, **74**, 59-65.

Zarrin, A., Sadighian, S., Rostamizadeh, K., Firuzi, O., Hamidi, M., Mohammadi-Samani, S. and Miri, R. (2016), "Design, preparation, and in vitro characterization of a trimodally-targeted nanomagnetic onco-theranostic system for cancer diagnosis and therapy", *Int. J. Pharm.*, **500**(1), 62-76.